Use of an Optical Dipole Trap in a Cold-atom Electron Source

Joshua Torrance

School of Physics

The University of Melbourne

October 5, 2012

Supervised by Robert Scholten

Abstract

Abstract text.

Statement of Contributions and Originality

No idea what this should look like. I should probably figure that out.

Contents

1

Introduction

The University of Melbourne's cold-atom electron source (CAES) project aims to create high-brightness, high-coherence electron bunches for use in coherent electron diffractive imaging. The imaging of nanoscale objects such as biological molecules [1,2] and defects in solid-state devices [3] by ultrafast, single-shot electron diffractive imaging could provide important information about structures and dynamic processes of important biological molecules such as membrane proteins.

1.1 Imaging of Bio-molecules

In order to determine the structure of biological molecules imaging techniques with atomics resolution are required. A number of techniques are capable of determining these structures [4–6] and the most successful to date has been x-ray crystallography [7,8]. Unfortunately the crystallisation process is difficult and to date only a small proportion of proteins have been successfully crystallised [9].

1.1.1 Membrane Proteins

Membrane proteins are the proteins that are associated with or attached to the membranes of cells. They are involved in detecting and conveying external signals into cells. This allows the cells to interact with and respond to their environment [10]. Membrane proteins are important in determining immune responses, interactions with pharmaceuticals, cell adhesion to form tissues and in controlling important metabolic processes such as salt balance, energy production and photosynthesis [11].

Determining the structure of theses molecules is a key step in understanding their chemical and biological function. The importance of knowing the atomic structure of biomolecules is exemplified by the enormous progress made in various fields of biology once the double-helical structure of DNA

was determined from x-ray images in 1953 [12]. Once a protein's structure and function are known then it becomes possible to design drugs [13] where needed and to more fully understand how the protein behaves in its biological system.

The developement of new imaging techniques, such as ultrafast single shot diffraction, and new light sources, such as x-ray free electron lasers (XFELs), have been driven by the goal of overcoming the limitations of x-ray crystallography. Ultrafast single-shot diffraction imaging also has the potential to able to determine the dynamic structure of biological molecules.

1.1.2 Ultrafast, single-shot, coherent diffractive imaging with electrons

X-ray diffraction from crystals was first observed a century ago [14] and resulted in a Nobel prize being awarded to William Bragg and his son. Since then coherent diffractive imaging (CDI) has been performed on a myriad of different samples with coherent beams of x-rays and electrons.

Ultrafast, single-shot imaging requires a very bright source of radiation in order to provide enough scattered information on the detector before the sample takes damage from the illumination [15]. Single-shot imaging with a sufficiently bright source and a short enough interaction time would be able to image protein molecules, and other bio-molecules, without the need for crystallisation [16].

With femtosecond timescale single-shot imaging it is possible to observe such things as molecular vibration and dynamic chemical processes [17]. With the sophisticated imaging techniques currently in development and the continued improvement of radiation sources it will become possible to create 'molecular movies' [1] of these processes.

Unfortunately, the brightnesses required for single shot imaging requires multi-billion-dollar XFEL facilities. Electron sources however may be able to provide cheaper alternatives. Electron interactions with molecules are significantly stronger than those of x-rays. For similar energies the electron interaction with a sample is $10^5 - 10^6$ times stronger than that of x-rays [18].

1.2 Melbourne cold-atom electron source

The University of Melbourne's CAES project aims to produce an electron source for coherent diffractive imaging. If bright, coherent, femtosecond long bunches of electrons can be produced then CDI can be performed on a range of structures and eventually molecules.

In order to produce the electrons Rubidium atoms are cooled and trapped in a retro-reflective magneto-optical trap (MOT) that is loaded from a Zeeman slower [19–21]. The valance electrons of the trapped atoms are ionised using a red (780 nm) and a blue (480 nm) laser.

The wavelength of the blue ionisation laser is tuned such that the electrons are given the

minimum energy required to ionise them ensuring that the electrons are 'cold' (approximately 10K [22]).

The cold electrons are accelerated out of the cloud by a uniform electric field generated by charged parallel plates, guided to the neighbouring sample chamber and focused onto the target sample. After passing through the sample the resulting diffraction pattern is incident upon the detector. The diffraction pattern recorded by the detector can be used to determine the structure of the sample using standard CDI techniques.

During the ionisation and acceleration stage the magnetic and optical trapping must be turned off. The optical trapping interferes with the exitation stage and the magnetic trapping would have extremely strong affects on the electron paths due to the low mass of the electrons. This means that, during these phases, the atom-cloud is no longer trapped and begins to expand and fall.

This cycle of trapping, ionisation, acceleration and imaging occurs with a frequency of 10 Hz during normal operation.

1.3 Stability of the cold-atom electron source

In its current state the CAES suffers from a number of technical issues that are preventing the observation of diffraction through samples. One of these issues is the stability of the atom-cloud and thus the electron signal.

The atom-cloud formed by the MOT has approximately 93 ms to fill which does not provide enough time for the trap to saturate. The distribution of the atoms within the cloud therefore varies from cycle to cycle. The atom distribution also varies during a single cycle as atoms 'slosh' within the trap. These issues are exacerbated when the trapping is turned off and the cloud begins to fall and expand.

This instability in the distribution of the atoms results in instability in the initial distribution of the electrons. This is apparent on the detector as shot-to-shot variations in the position of the electron beam. Removing this instability would make the application of imaging techniques more easier as well as providing more reliable use of the various electron optics in the system.

1.4 Optical dipole traps

Optical dipole traps (ODTs) may prove to be the solution to this stability problem. An ODT usually consists of a foccussed, Gaussian laser beam that is detuned from the atomic resonances of the target atomic species. The atoms feel a force towards the high intensity regions of the laser, ie. the centre of the beam and the focus.

1.4.1 History of optical dipole trapping

The use of the optical dipole force as a confining mechanism was first proposed by Askar'yan in 1962 [23] for plasmas and neutral atoms. Ashkin successfully demonstrated the trapping of micron-size latex spheres suspended in water using a focused Gaussian lasers in 1970 [24]. The first optical trapping of atoms was demonstrated by Chu et. al. in 1986 [25] where a ODT was used to trap sodium atoms.

Since then ODTs have been used extensively in atom optics especially in the creation of Bose-Einstein condensates (BECs) and atom lasers.

1.4.2 Optical dipole traps in the cold-atom electron source

The main advantage of ODT for the CAES is trapping without magnetic fields or on-resonance lasers. This means that the atom-cloud can remain trapped during the ionisation and acceleration phases of electron generation. This should reduce the current instability in the electron beam path.

ODT also provide the opportunity to experiment with other techniques such as evaporative cooling to compress the atom-cloud and optical lattices [26] to counter disorder induced heating.

ODTs used in the CAES must meet several criterion in order to be useful;

- The trap depth must be at least as deep as the temperature of the atoms in the MOT which is approximately 70 μK [22]. Making the trap ten times as deep as the target atoms seems like a good idea. why? citation The trap depth is affected by the power, detuning from resonance and size of the beam.

- The lifetime of the trap must be in excess of the length of the ionisation and acceleration phase which is not longer than 10ms. The lifetime of the trap is affected by the scattering rate of the trapping light field which is determined by the intensity of the light at the trap and the detuning from resonance.

- Ideally the size of the trap would encompass the entire MOT however this is impractical due to the laser power available. The minimum size of the trap should be the size of the excitation region which is approximately 500 μm [27].

2

Theory

2.1 MOT Physics

brief overview of zeeman slower, mot

2.2 Electron Generation in the Cold-Atom Electron Source

The CAES uses two stage photoionisation as its primary method of electron production. This method provides strong control over the excess energy of the ionised electrons which is essential to the production of cold electrons. Control of the initial electron bunch shape is also possible as described by McCulluch et. al. [22].

Two lasers with different wavelengths can be used for efficient ionisation of atoms while producing cold electrons. An excitation laser takes the atoms from the ground state to an intermediary excited state and an ionisation laser takes the excited atoms from the intermediary state to the ionisation continium. The excess energy of the ionised electrons can be controlled by varying the wavelength of the ionisation laser.

In the CAES the excitation laser is resonant to the D2 transition of the trapped ^{85}Rb atoms (780.24nm). This resonance results in efficient population transfer to the excited state. The ionisation laser can be set to couple the first excited state to a Rydberg state rather than to the ionisation continuum directly which results in resonant transitions. The resonant transition to a Rydberg state followed by field ionisation induced by the accelerating electric field (see figure 2.2) is more efficient than other ionisation pathways which rely on non-resonant behaviour. Field ionisation results in free electrons with very little energy ($T \approx 10K$ [22]) and are thus called 'cold'.

The cold electrons are then accelerated with an electric field and steered with a number of magnetic devices through the sample and onto the detector.

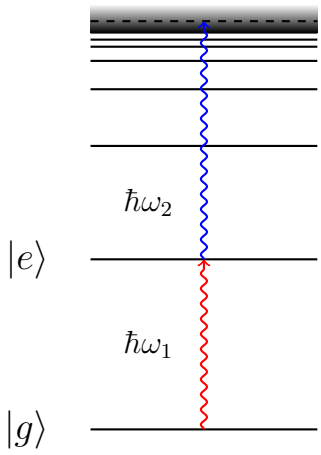

Figure 2.1: Energy level diagram for atom undergoing two-stage ionisation. Resonant excitation from the ground state, $|g\rangle$ to the excited state $|e\rangle$ is achieved with a coupling laser of frequency ω_1. A second laser of frequency ω_2 is used to couple $|e\rangle$ to the ionisation continuum. Changing ω_2 allows the excess energy of the ionisation process to be adjusted.

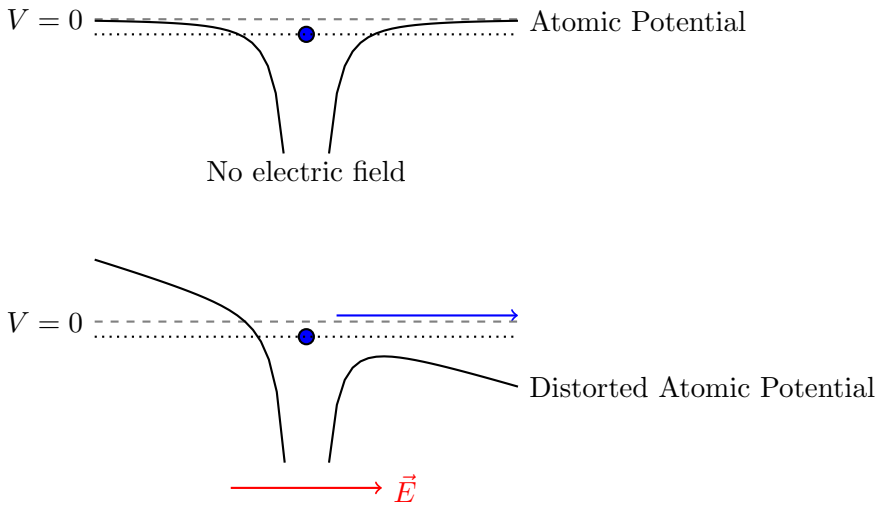

Figure 2.2: The top diagram dipicts an atom excited to a Rydberg state without the presence of an electric field. The lower diagram show the same atom in the presence of an electric field. The electric field distorts the atomic potential in such a way as to allow the atom to become ionised. The solid black lines represent the atomic potential, the dashed lines the zero field ionisation threshhold, the dotted lines the energy of the valence electrons, the blue circles show the elctrons and the red arrow the direction of the electric field.

2.3 Optical Dipole Traps

The following derivation of the dipole potential and scattering rate for ODT follows the one presented in Grimm and Weidemüller [28].

An electric field, E, from laser light of frequency ω will induce an atomic dipole moment $\boldsymbol{p}$ in an atom placed within the light field. Using standard complex notation we can write,

$$\boldsymbol{E}(\boldsymbol{r},t) = \hat{\boldsymbol{e}}\tilde{E}(\boldsymbol{r}) \exp -i\omega t + c.c. \tag{2.1}$$

where $\hat{\boldsymbol{e}}$ is the polarisation unit vector. The amplitude of the dipole moment, $\tilde{p}$, is related to the electric field amplitude, $\tilde{E}$, by

$$\tilde{p} = \alpha\tilde{E}. \tag{2.2}$$

α depends on the driving frequency, ω and is called the complex polarisability.

The induced dipole moment, $\boldsymbol{p}$ has an interaction potential with the electric field, $\boldsymbol{E}$ given by

$$U_{dip} = -\frac{1}{2}\langle \boldsymbol{pE}\rangle = -\frac{1}{2\epsilon_0 c} Re(\alpha) I, \tag{2.3}$$

where the time average over the rapidly oscillating terms is indicated by the angle brackers, the field intensity is $I = 2\epsilon_0 c|\tilde{E}|^2$ and the $\frac{1}{2}$ takes the the induced nature of the dipole moment in account. The dipole force results from the gradient of the interaction potential

$$\boldsymbol{F}_{dip}(\boldsymbol{r}) = -\nabla U_{dip}(\boldsymbol{r}) = \frac{1}{2\epsilon_0 c} Re(\alpha)\nabla I(\boldsymbol{r}). \tag{2.4}$$

The dipole force is a conservative force and is proportional to gradient of the intensity of the light field.

The oscillator absorbs power from the light field which is re-emitted as dipole radiation. This is given by,

$$P_{abs} = \langle \dot{\boldsymbol{p}}\boldsymbol{E}\rangle = 2\omega Im(\tilde{p}\tilde{E}^*) = \frac{\omega}{\epsilon_0 c} Im(\alpha) I \tag{2.5}$$

The complex part of the polarisability gives the out of phase component of the dipole oscillation which results in absorption. Absorption can be interpreted in terms of photon scattering in cycles of absorption and emission of photons of energy $\hbar\omega$. This corresponds to a scattering rate of

$$\Gamma(\boldsymbol{r}) = \frac{P_{abs}}{\hbar\omega} = \frac{1}{\hbar\epsilon_0 c} Im(\alpha) I(\boldsymbol{r}). \tag{2.6}$$

2.3.1 Atomic Polarisability

The atomic polarisability, α can be calculated by using Lorentz's model for a classical oscillator citation please. In this picture an electron with mass m_e and charge e is considered to be bounds to the core elastically with an oscillation frequency ω_0 which corresponds to the optical transition frequency.

The polarisability can be calculated if the equation of motion, $\ddot{x} + \gamma\dot{x} + \omega_0^2 x = -eE(t)/m_e$, is integrated for the driven oscillation of the electron to give

$$\alpha = \frac{e^2}{m_e}\frac{1}{\omega_0^2 - \omega^2 - i\omega\Gamma_\omega} \tag{2.7}$$

where the damping rate due to radiative energy loss is

$$\Gamma_\omega = \frac{e^2\omega^2}{6\pi\epsilon_0 m_e c^3}. \tag{2.8}$$

By substituting $e^2/m_e = 6\pi\epsilon_0 c^3\Gamma_\omega/\omega^2$ and the on-resonance damping rate $\Gamma \equiv \Gamma_{\omega_0} = (\omega_0/\omega)^2\Gamma_\omega$ we get

$$\alpha = 6\pi\epsilon_0 c^3 \frac{\Gamma/\omega_0^2}{\omega_0^2 - \omega^2 - i(\omega^3/\omega_0^2)\Gamma} \tag{2.9}$$

While this is classically derived is serves as a good approximation for far-detuned dipole traps due to the relatively low scattering rates and hence low saturation [28].

2.3.2 Optical Dipole Force and Scattering Rate

Using equation 2.9 in 2.3 and 2.6 in the case of large detuning and negligible saturation we can derive

$$U_{dip}(\boldsymbol{r}) = -\frac{3\pi c^2}{2\omega_0^3}\left(\frac{\Gamma}{\omega_0 - \omega} + \frac{\Gamma}{\omega_0 + \omega}\right) I(\boldsymbol{r}), \tag{2.10}$$

and

$$\Gamma_{sc} = \frac{3\pi c^2}{2\hbar\omega_0^3}\left(\frac{\omega}{\omega_0}\right)^3\left(\frac{\Gamma}{\omega_0 - \omega} + \frac{\Gamma}{\omega_0 + \omega}\right)^2 I(\boldsymbol{r}). \tag{2.11}$$

Most experiments are performed with ω relatively close to the resonance, ω_0. In this case the detuning $\Delta \equiv \omega - \omega_0 \ll \omega_0$. Here we can make the rotating wave approximation and set $\omega/\omega_0 \approx 1$. The equations above simplify to

$$U_{dip}(\boldsymbol{r}) = \frac{3\pi c^2}{2\omega_0^3}\frac{\Gamma}{\Delta} I(\boldsymbol{r}), \tag{2.12}$$

and

$$\Gamma_{sc}(\boldsymbol{r}) = \frac{3\pi c^2}{2\hbar\omega_0^3}\left(\frac{\Gamma}{\Delta}\right)^2 I(\boldsymbol{r}). \tag{2.13}$$

These equations provide the basis for understanding the operation of dipole traps. The sign of the detuning is clearly important. For below resonance or 'red' detuning ($\Delta < 0$) the dipole potential is negative and atoms are drawn into the high intensity portions of the light field. Above resonance or 'blue' detuning ($\Delta > 0$) results in repulsion from the high intensity regions of the light and a positive potential.

The potential scales with I/Δ and the scattering scales with I/Δ^2 which means that for a certain potential depth high intensity and detuning will result in the least scattering.

As previously mentioned Gaussian beams are used for red-detuned ODTs. A Gaussian beam's intensity $I(r, z)$ at a given radius r from the beam centre and distance from the focus z can be defined as [29]

$$I(r, z) = I_0\left(\frac{w_0}{w(z)}\right)^2 e^{-2r^2/w(z)^2} \tag{2.14}$$

where I_0 is the intensity at the centre of the focal point, w_0 is the beam waist at the focus and the beam waist $w(z)$ is

$$W(z) = \sqrt{1 + \left(\frac{z}{z_0}\right)^2}. \tag{2.15}$$

Here z_0 is the Rayleigh length and is given by

$$z_0 = \frac{\pi w_0^2}{\lambda}. \tag{2.16}$$

Gaussian beam diagram? ¡- only if time permits

These equations can be used to simulate an ODT. Using the light sources similar to those described in chapter 3 we can create generate the potential depicted in figure 2.3.2. The potential has been converted to an effective temperature, T_{eff} using

$$T_{eff}(r, z) = \frac{2}{3k_B}U(r, z) \tag{2.17}$$

where U is the potential and k_B is Boltzmann's constant.

Still need to talk about how these equations make a trap as well as some theoretical numbers

2.3.3 lifetime

hmmm what to do here....

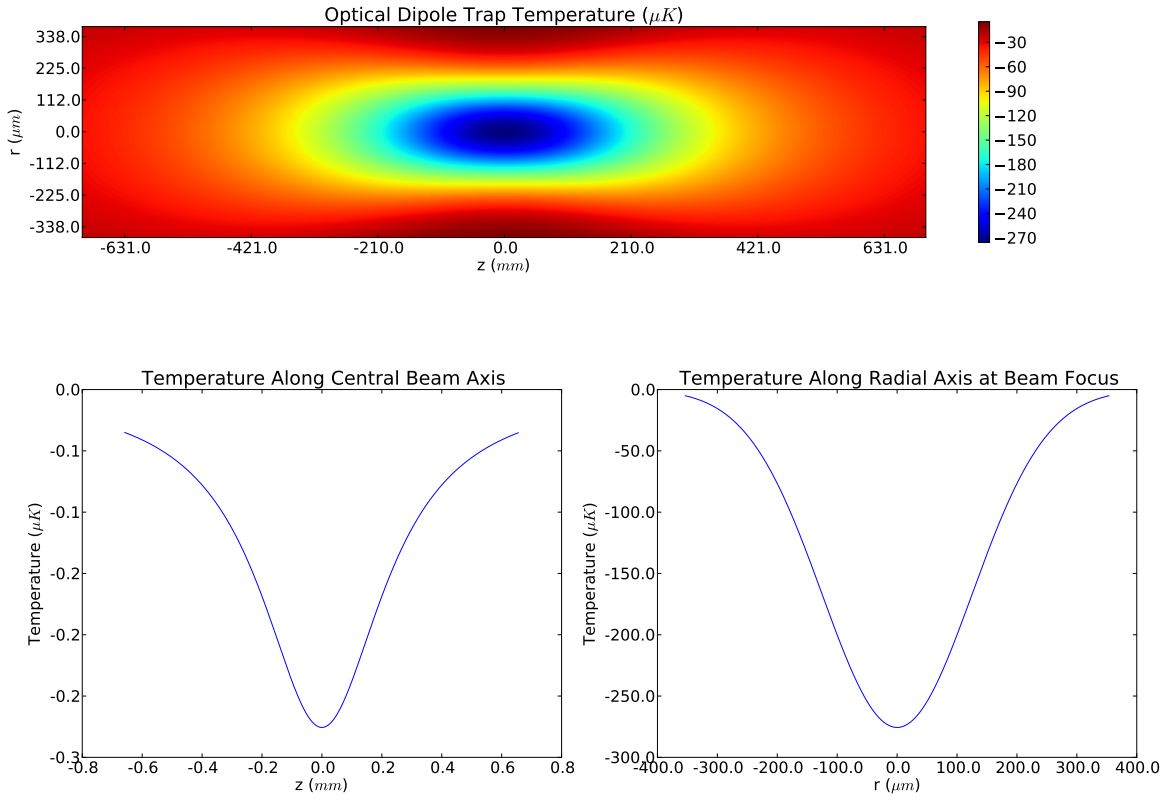

Figure 2.3: The effective temperature of a single beam optical dipole trap is depicted here. The total power of the simulated beam is 500mW with a detuning of 2nm red of the 85Rb D2 resonance and a beam waist of 250μm. The top graph shows a cross section through the centre of the beam (note that the scale and units on each axis are different). The graph on the bottom left shows the effective temperature along the r=0 axis and the graph on the right shows the temperature along the z=0 axis.

2.3.4 Configuration

The simplest form of optical dipole trap consists of a single focussed Gaussian beam that can trap atoms at the focus. These simple traps have been used since the 1980s [25] and are frequently used to form BECs and atom lasers [30–32].

Single beam traps have strong confinement in the direction perpendicular to the beam and relatively weak confinement along the beam. A trap with strong confinement in all directions can be created by crossing two beams. Crossed beam traps are used frequently to produce BECs [33–37].

diagram!

remember to mention polarisation stuff for the crossed beam trap

2.4 Imaging

In order to determine the spatial distribution of the atoms at a given time techniques for imaging are required. Numerous techniques for imaging are available the simplest of which are fluorescence and absorption imaging.

2.4.1 Fluorescence Imaging

Near resonant light passing through atom clouds (such as the optical mollasses lasers in a MOT or a specific probe beam) will be absorbed and re-emitted in a random direction. These scatter photons can be easily detected and images of the scattered photons can be easily produced. This method is easy to do and has the advantage that imaging can be done on any axis. The signal is rather weak however since the scattered photons are equally distributed in all directions so only a small portion will reach the detector. Due to the strong interaction of the laser light with the atoms this is a destructive imaging method.

diagram i should probably define destructive and non-destructive imaging methods

Fluorescence imaging is very easy to accomplish with the Melbourne CAES when used to view the MOT due to the fluorescence from the cooling lasers. However it is not practical for use with atoms trapped in an ODT since with the significantly reduced atom count the signal from fluorescence imaging will not be detectable.

2.4.2 Absorption Imaging

Absorption imaging is another destructive imaging method that makes use of an on-resonance probe laser. In absorption imaging a collimated probe laser is directed through the atoms and onto the detector. As in fluorescence imaging the photons will be absorbed and reemitted in

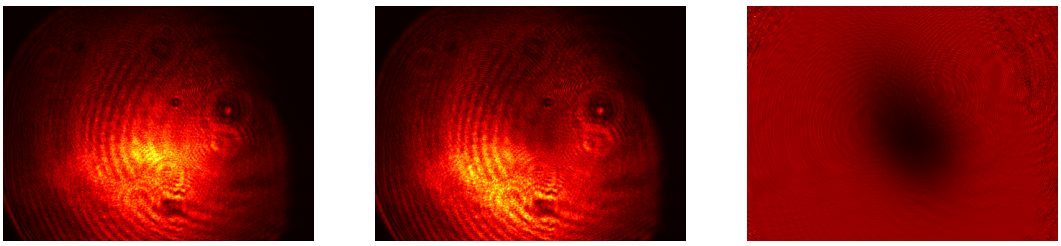

Figure 2.4: The above images are an example of absorption imaging. The image on the left is that of the on-resonance probe beam taken while the magnetic trapping of the magneto-optic trap was turned off and no atoms were trapped. The centre image shows the probe beam after it had passed through the atom-cloud of the normal magneto-optic trap and the corresponding shadow is clearly visible. The transmission function of the atoms (see equation 2.18) is shown in the right image.

random directions. After the light has passed through the atoms a 'shadow' due to the photons absorbed by the atoms will be left in the probe beam.

diagram

The signal from absorption imaging is much stronger than that for fluorescence however it is not possible to get quantitative information for dense clouds of atoms due to the exponential drop in transmission [38]. This is not a problem for the atoms trapped in the CAES since no compression is currently being used on the MOT or ODT.

The strong interaction between the laser and the atoms means that with a 'fragile' trap this imaging technique will give many of the atoms enough energy to escape the trap.

Absorption Imaging Analysis

If I_0 is an image of the probe beam taken while there are no atoms present and I is an image of the probe beam with the atoms present then the transmission function for the atoms, T, can be calculated with

$$I = TI_0. \tag{2.18}$$

Each point in T corresponds to the integrated column density of the atoms in the cloud at that point and this information can be used to determine a number of different metrics such as the temperature of the atoms and the total number of atoms.

MOT Temperature

An atomic distribution in an ideal MOT atom cloud should be a Gaussian distribution whose two dimensional density can be modeled by

$$\rho(x,y) = \rho_0 \exp\left(\frac{x^2}{\sigma_x^2} + \frac{y^2}{\sigma_y^2}\right) \tag{2.19}$$

where ρ_0 is the central density and σ_x and σ_y are the 1/e radii of the distribution.

If the trapping lasers and magnetic fields are turned off the atom-cloud should begin to expand thermally. The r.m.s thermal velocity, v_0, is related to the temperature of the cloud, T, via [39]

$$v_0 = \sqrt{\frac{2k_B T}{m_{Rb}}} \tag{2.20}$$

where k_B is Boltzmann's constant and m_{Rb} is the mass of rubidium. The radius of the atom cloud, r, at time t after it has been released is given by

$$r(t) = \sqrt{r_0^2 + (v_0 t)^2}. \tag{2.21}$$

Here r_0 is the initial 1/e spatial radius of the cloud.

The temperature can be calculated by taking a number of absorption images for various values of t and then fitting each of the atomic distributions to equation 2.19. The various cloud radii can then be fitted to equation 2.21 and a temperature can then be calculated with equation 2.20.

Atom Count

It is useful to know the number of atoms in a given absorption image. To do this we need to know the magnification of the optical system in front of the detector as well as the power of the probe laser.

As the probe laser traverses through the atoms cloud its intensity obeys Beer's lawcitation,

$$I(x,y) = I_0(x,y)e^{-D(x,y)} \tag{2.22}$$

where $I_0(x,y)$ is the intensity of the beam before the cloud, $I(x,y)$ is the intensity after the cloud and $D(x,y)$ is the optical depth along the probe beam's axis. The coordinates (x,y) denote a given position in the plane perpendicular to the probe beam. The optical density is given bycitation

$$D(x,y) = \sigma \int_{-\infty}^{\infty} n(x,y,z)dz. \tag{2.23}$$

Here σ is the absorption cross-section and $n(x, y, z)$ is the atomic density distribution. The details of $n(x, y, z)$ are unimportant for many applications where only the total number of atoms, N, is required.

Using equations 2.22 and 2.23 we can get

$$D(x, y) = -\log_e(\frac{I}{I_0}) = \sigma \int_{-\infty}^{\infty} n(x, y, z)dz. \tag{2.24}$$

By integrating across the image we obtain

$$\int_{-\infty}^{\infty}\int_{-\infty}^{\infty} \frac{1}{\sigma} D(x, y)dxdy = N. \tag{2.25}$$

Practically I, I_0 and $D(x, y)$ will be two dimensional arrays of pixels, so The integrals can be written as sums giving

$$N = A \sum_{(x,y)} \frac{1}{\sigma} D(x, y) \tag{2.26}$$

where A is the scaled area of the detector.

The absorption cross-section is given by [40],

$$\sigma = \frac{\sigma_0}{1 + 4(\Delta/\Gamma)^2 + (I/I_s)} \tag{2.27}$$

where Δ is the frequency detuning of the pump light ($\Delta = 0$ for on-resonant light) and σ_0 is the on-resonance, low-intensity cross-section

$$\sigma_0 = \frac{\hbar\omega\Gamma}{2I_s}. \tag{2.28}$$

If on-resonant light with an intensity much less than the saturation intensity is used $\sigma \approx \sigma_0$ and

$$N = -\frac{A}{\sigma_0} \sum_{(x,y)} \log_e \left(\frac{I(x, y)}{I_0(x, y)} \right). \tag{2.29}$$

If the low-intensity condition is not satisfied then the following must be used

$$N = -A \sum_{(x,y)} \frac{1 + (I(x, y)/I_s)}{\sigma_0} \log_e \left(\frac{I(x, y)}{I_0(x, y)} \right). \tag{2.30}$$

The pixel scale factor can be calculated by placing an object with known dimensions (such as a ruler) at the object plane and then determining the number of pixels taken up by the object. Simply multiplying the pixel scale factor squared by the area of the probe beam on the detector to get A.

2.4.3 Other Imaging Methods

There are a number of other imaging techniques that can be used to image cold-atom clouds some of which are destructive and some are non-destructive. The non-destructive methods are particularly useful for imaging delicate systems such as BECs. An example of a minimally destructive technique is diffractive contrast imaging [41]. There are other techniques such as diffractive dark-ground imaging [42] and phase contrast imaging [43]. Each of these techniques has it's own useful properties but few are as simple to setup and perform as absorption and fluorescence imaging.

2.5 Trap Stability

not sure what to do here - might drop this section

2.6 Stability of the Electron Signal

The stability of the electron signal incident on the detector can be analysed fairly simple. For a given iteration, i, of the experiment the electron signal will have an average spatial centre given by

$$\boldsymbol{x}_i = \frac{1}{\sum c(p)} \sum c(p)\boldsymbol{x}(p) \tag{2.31}$$

where both sums are over all the pixels, p, of the detector, $c(p)$ are the counts for a given pixel and $\boldsymbol{x}(p)$ are the locations of each pixel.

The average of a set of measurements, $\bar{\boldsymbol{x}}$, and the associated variance, μ, for a set of size n are given by

$$\bar{\boldsymbol{x}} = \frac{1}{n}\sum_{i=0}^{n} \boldsymbol{x}_i \tag{2.32}$$

$$\mu^2 = \frac{1}{n}\sum_{i=0}^{n} (\boldsymbol{x}_i - \bar{\boldsymbol{x}})^2 \tag{2.33}$$

These simple calculations can be used to analyse the spatial variation of the electron signal and the variance can be used as a metric for determining whether the stability of the source is being improved by changes.

any other cunning stats tricks for this?

3

Experiment

The CAES at the University of Melbourne has be assembled over a number of years. The experimental cycle can be divided into several parts which will be descibed in this chapter. More details of the various experimental apparatus can be found in the groups recent papers [22] MOAR papers please and theses [27, 39, 44].

3.1 main setup

mot etc

3.2 TA

3.3 Fiber laser

3.4 dipole rig

3.5 absorption imaging

3.6 magnetic tentacle monster

4

Results

If I ever get any results go in here.

4.1 magnetic control

get some current displacement numbers

4.2 absorption images of the mot

4.2.1 metrics

4.3 absorption images of ODT

4.3.1 metrics

Glossary

BEC Bose-Einstein condensate.

CAES cold-atom electron source.

CDI coherent diffractive imaging.

MOT magneto-optical trap.

ODT optical dipole trap.

XFEL x-ray free electron laser.

Bibliography

[1] J. R. Dwyer, C. T. Hebeisen, R. Ernstorfer, M. Harb, V. B. Deyirmenjian, R. E. Jordan, and R. J. Dwayne Miller. Femtosecond electron diffraction: 'making the molecular movie'. *Philosophical Transactions of the Royal Society A: Mathematical, Physical and Engineering Sciences*, 364(1840):741–778, March 2006. 1, 2

[2] J. C. Williamson, J. Cao, H. Ihee, H. Frey, and A. H. Zewail. Clocking transient chemical changes by ultrafast electron diffraction. *Nature*, 386(6621):159–162, March 1997. 1

[3] B. J. Siwick, J. R. Dwyer, R. E. Jordan, and R. J. Dwayne Miller. An atomic-level view of melting using femtosecond electron diffraction. *Science*, 302(5649):1382–1385, November 2003. 1

[4] J. E Nettleship, J. Brown, M. R. Groves, and A. Geerlof. Methods for protein characterization by mass spectrometry, thermal shift (ThermoFluor) assay, and multiangle or static light scattering. *Methods in Molecular Biology (Clifton, N.J.)*, 426:299–318, 2008. PMID: 18542872. 1

[5] D. I. Svergun and M. H. J. Koch. Small-angle scattering studies of biological macromolecules in solution. *Reports on Progress in Physics*, 66(10):1735–1782, October 2003. 1

[6] S. J. Opella and F. M. Marassi. Structure determination of membrane proteins by NMR spectroscopy. *Chemical Reviews*, 104(8):3587–3606, August 2004. PMID: 15303829. 1

[7] J. C. Kendrew, G. Bodo, H. M. Dintzis, R. G. Parrish, H. Wyckoff, and D. C. Phillips. A three-dimensional model of the myoglobin molecule obtained by x-ray analysis. *Nature*, 181(4610):662–666, March 1958. 1

[8] I. Usón and G. M. Sheldrick. Advances in direct methods for protein crystallography. *Current Opinion in Structural Biology*, 9(5):643–648, October 1999. PMID: 10508770. 1

[9] A. Geerlof, J. Brown, B. Coutard, M. P. Egloff, F. J. Enguita, M. J. Fogg, R. J. C. Gilbert, M. R. Groves, A. Haouz, J. E. Nettleship, P. Nordlund, R. J. Owens, M Ruff, S. Sainsbury, D. I.

Svergun, and M. Wilmanns. The impact of protein characterization in structural proteomics. *Acta Crystallographica. Section D, Biological Crystallography*, 62(Pt 10):1125–1136, October 2006. PMID: 17001090. 1

[10] M. S. Almén, K. J. V. Nordström, R. Fredriksson, and H. B. Schiöth. Mapping the human membrane proteome: a majority of the human membrane proteins can be classified according to function and evolutionary origin. *BMC Biology*, 7(1):50, August 2009. 1

[11] D. D. Chiras. *Human Biology*. Jones & Bartlett Learning, August 2011. 1

[12] J. D. Watson and F. H. C. Crick. Molecular structure of nucleic acids: A structure for deoxyribose nucleic acid. *Nature*, 171(4356):737–738, April 1953. 2

[13] L. H. Pinto, L. J. Holsinger, and R. A. Lamb. Influenza virus m2 protein has ion channel activity. *Cell*, 69(3):517–528, May 1992. 2

[14] W. H. Bragg. X-rays and crystals. *Nature*, 90:219, October 1912. 2

[15] R. Henderson. The potential and limitations of neutrons, electrons and x-rays for atomic resolution microscopy of unstained biological molecules. *Quarterly Reviews of Biophysics*, 28(2):171–193, May 1995. PMID: 7568675. 2

[16] R. Neutze, R. Wouts, D. van der Spoel, E. Weckert, and J. Hajdu. Potential for biomolecular imaging with femtosecond x-ray pulses. *Nature*, 406(6797):752–757, August 2000. 2

[17] A. H. Zewail. 4d ultrafast electron diffraction, crystallography, and microscopy. *Annual Review of Physical Chemistry*, 57(1):65–103, 2006. 2

[18] G. Sciaini and R. J. Dwayne Miller. Femtosecond electron diffraction: heralding the era of atomically resolved dynamics. *Reports on Progress in Physics*, 74(9):096101, September 2011. 2

[19] William D. Phillips and Harold Metcalf. Laser deceleration of an atomic beam. *Physical Review Letters*, 48(9):596–599, March 1982. 2

[20] William D. Phillips and Harold J. Metcalf. Cooling and trapping atoms. *j-SCI-AMER*, 256(3):36–42, March 1987. 2

[21] S C Bell, M Junker, M Jasperse, L D Turner, Y-J Lin, I B Spielman, and R E Scholten. A slow atom source using a collimated effusive oven and a single-layer variable pitch coil zeeman slower. *The Review Of Scientific Instruments*, 81(1):013105, January 2010. 2

[22] A. J. McCulloch, D. V. Sheludko, S. D. Saliba, S. C. Bell, M. Junker, K. A. Nugent, and R. E. Scholten. Arbitrarily shaped high-coherence electron bunches from cold atoms. *Nature Physics*, 7(10):785–788, July 2011. 3, 4, 5, 17

[23] G. Askar'yan. Effects of the gradient of a strong electromagnetic beam on electrons and atoms. *Soviet Physics - Journal of Experimental and Theoretical Physics*, 15(1088), 1962. INSPEC:10786990. 4

[24] A. Ashkin. Acceleration and trapping of particles by radiation pressure. *Physical Review Letters*, 24(4):156–159, January 1970. 4

[25] S. Chu, J. E. Bjorkholm, A. Ashkin, and A. Cable. Experimental observation of optically trapped atoms. *Physical Review Letters*, 57(3):314–317, July 1986. 4, 11

[26] Leonardo Fallani, Chiara Fort, Jessica Lye, and Massimo Inguscio. Bose-einstein condensate in an optical lattice with tunable spacing: transport and static properties. *Optics express*, 13(11):4303–4313, May 2005. PMID: 19495345. 4

[27] A. J. McCulloch. *Electron diffraction from a cold atom electron source*. Unpublished doctoral dissertation, The University of Melbourne, Melbourne, Australia, 2012. 4, 17

[28] R. Grimm, M. Weidemüller, Y. B. Ovchinnikov, Benjamin Bederson, and Herbert Walther. Optical dipole traps for neutral atoms. In *Advances In Atomic, Molecular, and Optical Physics*, volume Volume 42, pages 95–170. Academic Press, 2000. 7, 8

[29] Bahaa E. A. Saleh and Malvin Carl Teich. *Fundamentals of photonics*. Wiley-Interscience, February 2007. 9

[30] A. P. Chikkatur, Y. Shin, A. E. Leanhardt, D. Kielpinski, E. Tsikata, T. L. Gustavson, D. E. Pritchard, and W. Ketterle. A continuous source of bose-einstein condensed atoms. *Science*, 296(5576):2193–2195, June 2002. 11

[31] G. Kleine Büning, J. Will, W. Ertmer, C. Klempt, and J. Arlt. A slow gravity compensated atom laser. *Applied Physics B: Lasers and Optics*, 100(1):117–123, 2010. 11

[32] Y.-J. Lin, A. R. Perry, R. L. Compton, I. B. Spielman, and J. V. Porto. Rapid production of $ˆ87$rb bose-einstein condensates in a combined magnetic and optical potential. *Physical Review A*, 79(6):063631, June 2009. 11

[33] A. Couvert, M. Jeppesen, T. Kawalec, G. Reinaudi, R. Mathevet, and D. Guéry-Odelin. A quasi-monomode guided atom laser from an all-optical bose-einstein condensate. *EPL (Europhysics Letters)*, 83(5):50001, September 2008. 11

[34] K. J. Arnold and M. D. Barrett. All-optical Bose–Einstein condensation in a 1.06 \mu m dipole trap. *Optics Communications*, 284(13):3288–3291, June 2011. 11

[35] Zhengkun Fu, Pengjun Wang, Shijie Chai, Lianghui Huang, and Jing Zhang. Bose-einstein condensate in a light-induced vector gauge potential using 1064-nm optical-dipole-trap lasers. *Physical Review A*, 84(4):043609, October 2011. 11

[36] M. D. Barrett, J. A. Sauer, and M. S. Chapman. All-optical formation of an atomic bose-einstein condensate. *Physical Review Letters*, 87(1):010404, June 2001. 11

[37] D. Xiong, P. Wang, Z. Fu, S. Chai, and J. Zhang. Evaporative cooling of 87Rb atoms into bose-einstein condensate in an optical dipole trap. *Chinese Optics Letters*, 8(7):627–629, July 2010. 11

[38] David Moravchik. *Imaging Methods of Cold Atoms*. MSc thesis, Ben-Gurion University of the Negev, January 2009. 12

[39] David V Sheludko. *Shaped Electron Bunches from Ultracold Plasma*. PhD thesis, The University of Melbourne, Melbourne, Australia, December 2010. 13, 17

[40] D. A. Steck. *Rubidium 87 D line data*. 2001. 14

[41] David V Sheludko, Simon C Bell, Edgar J D Vredenbregt, and Robert E Scholten. Excited-state imaging of cold atoms. *Journal of Physics: Conference Series*, 80:012040, September 2007. 15

[42] Konstantinidis Gregory-Orfeus. *Diffractive Dark-Ground Imaging of Ultra-Low Atom-Numbers in a MOT*. PhD thesis, University of Crete, December 2011. 15

[43] M. R. Andrews, D. M. Kurn, H.-J. Miesner, D. S. Durfee, C. G. Townsend, S. Inouye, and W. Ketterle. Propagation of sound in a bose-einstein condensate. *Physical Review Letters*, 79(4):553–556, July 1997. 15

[44] S. D. Saliba. *Partially coherent electron diffractive imaging using an ultracold plasma based source*. PhD thesis, The University of Melbourne, Melbourne, Australia, March 2011. 17